Vortical Flows over a Delta Wing at High Angles of Attack

Young-Ki Lee, Heuy-Dong Kim*
School of Mechanical Engineering, Andong National University,
388 Songcheon-dong, Andong, Kyeongbuk, 760-749, Korea

The vortex flow characteristics of a sharp-edged delta wing at high angles of attack were studied using a computational technique. Three dimensional, compressible Reynolds-averaged Navier-Stokes equations were solved to understand the effects of the angle of yaw, angle of attack, and free stream velocity on the development and interaction of vortices and the relationship between suction pressure distributions and vortex flow characteristics. The present computations gave qualitatively reasonable predictions of vortical flows over a delta wing, compared with past wind tunnel measurements. With an increase in the angle of yaw, the symmetry of the pair of leading edge vortices was broken and the vortex strength was decreased on both windward and leeward sides. An increase in the free stream velocity resulted in stronger leading edge vortices with an outboard movement.

Key Words: Angle of Attack, Angle of Yaw, Delta Wing, Vortical Flow, Vortex Breakdown

Nomenclature

C_p : Static pressure coefficient
c : Chord length
E : Total energy per unit mass
H : Total enthalpy per unit mass
k : Turbulent kinetic energy
Pr_t : Turbulent Prandtl number
p : Pressure in pascal
s : Local semi-span
t : Time
T : Temperature in Kelvin
u_i : Velocity in ith direction
u_i' : Velocity fluctuation in ith direction
V : Free stream velocity
x_i : Coordinates in ith direction
ε : Turbulent dissipation rate
α : Angle of attack
β : Angle of yaw
κ : Thermal conductivity
μ : Viscosity
μ_t : Turbulent viscosity
ρ : Density
τ_{ij} : Deviatoric stress tensor

* Corresponding Author,
E-mail : kimhd@andong.ac.kr
TEL : +82-54-820-5622; **FAX** : +82-54-823-5495
School of Mechanical Engineering, Andong National University, 388 Songcheon-dong, Andong, Kyeongbuk, 760-749, Korea. (Manuscript **Received** March 2, 2002; **Revised** September 27, 2003)

1. Introduction

Many modern supersonic aircraft, especially fighters, requiring high maneuverability have preferably adopted delta wings in order to minimize the influence of the shockwave generated on wing surfaces and thus to maintain stability at supersonic speeds. At low speeds and high angles of attack, however, delta wings can introduce detrimental aerodynamic problems such as a sudden reduction of maneuverability and generation of induced drag. Moreover, these generally have considerable difficulties in the use of high-lift devices like a flap and special care needs to be taken to avoid stall at take-off or landing with high angle of attacks (Erickson et al., 1989; Ekaterinaris and Schiff, 1993).

Figure 1 shows a typical subsonic flowfield over the upper surface of a delta wing with a free stream velocity of V and an angle of attack of α. Relatively higher pressure on the bottom plane causes the flow in the vicinity of the leading

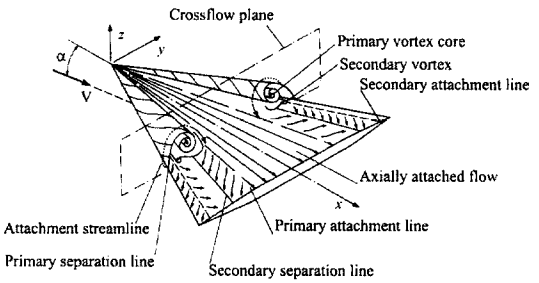

Fig. 1 Schematic diagram of the subsonic flowfield over a delta wing

edge to roll up towards the top plane. Then the rotating flow separates from the wing due to the effect of the sharp leading edge and produces a primary vortex. As shown in the figure, the flow reattaches along the primary attachment line and then secondarily separates and reattaches below the primary vortex, forming an oppositely rotating secondary vortex (Hummel, 1978). The leading-edge vortex consequently dominates the overall flowfields on the delta wing. At moderate to high angles of attack, the vortices induce large suction on the wing and thus produce a significant vortex-lift increment. Beyond a critical angle of attack, however, the vortices undergo a sudden expansion, called vortex breakdown (Wentz and Kohlman, 1971) resulting in a significant loss of lift, a sudden change of pitching moment and buffeting.

Since the 1950s, in order to understand the flow physics around various types of delta wings at high angles of attack, considerable effort has been made through experimental and numerical methodologies. Verhaagen et al.(1989) studied the influence of yaw on the flows over a sharp-edged biconvex delta wing at a constant angle of attack of 21.1° through laserlight sheet and oil-flow visualization techniques, and pressure and force balance measurements. Grismer et al. (1995) experimentally investigated the aerodynamic characteristics of a yawed delta wing with the strake at both static and sinusoidally varying angles of attack. Lowson et al.(1995) examined the effects of delta wing configurations, especially apex geometries, on the position of vortex breakdown. Lee and Sohn (2003) investigated the vortical flows over a delta wing with a leading edge extension through wing-surface pressure measurements, off-surface flow visualizations and 5-hole probe measurements of a wing wake section. Recently, several Navier-Stokes computations (Fujii and Schiff, 1989; Ekaterinaris and Schiff, 1990; Ken, 1993; Robinson et al., 1994; Görtz et al., 1999) have been conducted to predict separation and vortex breakdown and to find practical control techniques of these phenomena. These studies provided a good understanding of the flow features existing around yawed delta wings or double-delta wings. The experimental studies, however, could not provide comprehensive data to examine the detailed physics of vortical flow due to the difficulty in visualizing the flow structure. Furthermore, there have been rather limited numerical studies which can give quantitative information regarding the vortical flow and its relation to the aerodynamic load characteristics of the yawed delta wings at high angles of attack.

In the present study, three-dimensional compressible Reynolds-averaged Navier-Stokes simulations were carried out to give a detailed understanding of the vortex flow characteristics of a simple sharp-edged delta wing with and without yaw at angles of attack. The results obtained from the present computations were compared with the experimental data (Sohn and Lee, 2002; Kim et al., 2003) and gave the visualization of path lines, density and total pressure contours, vorticity, particle trajectory, etc. which were costly and hardly to be obtained by experimental work.

2. Model Configuration

Figure 2 shows the schematic diagram of the delta wing model tested in the present CFD analysis and it is taken from the past reports (Sohn and Lee, 2002; Kim et al., 2003) for comparison. The present wing model is a flat type wing with a chord of 600 mm, a span of 475.4 mm at the trailing edge, a sweepback angle of 65° and a thickness of 15 mm. The leading edge of wing has a bevel angle of 25°. In the

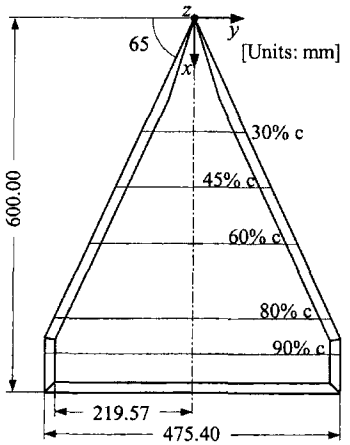

Fig. 2 Schematic diagram of delta wing model

Cartesian coordinate system, x is the chordwise distance along the wing centerline measured from the wing apex, y is the spanwise distance measured from the wing centerline, and z is the normal distance to the wing upper surface. The origin of the coordinate system is the apex of the delta wing and five representative chord locations are given to observe vortex development.

3. Numerical Simulations

3.1 Governing equations

Three-dimensional Reynolds-averaged Navier-Stokes and energy equations governing the flowfield around delta wings are given in differential form as follows;

$$\frac{\partial \rho}{\partial t}+\frac{\partial}{\partial x_i}(\rho u_i)=0 \tag{1}$$

$$\frac{\partial}{\partial t}(\rho u_i)+\frac{\partial}{\partial x_j}(\rho u_i u_j)=\frac{\partial}{\partial x_j}\mu\left(\frac{\partial u_i}{\partial x_j}+\frac{\partial u_j}{\partial x_i}\right)-\frac{\partial}{\partial x_i}\left(\frac{2}{3}\mu\frac{\partial u_l}{\partial x_l}\right)-\frac{\partial p}{\partial x_i}+\frac{\partial}{\partial x_j}(-\rho\overline{u_i' u_j'}) \tag{2}$$

$$\frac{\partial}{\partial t}(\rho E)+\frac{\partial}{\partial x_i}(\rho u_i H)=\frac{\partial}{\partial x_i}\left[\left(\kappa+\frac{\mu_t}{\mathrm{Pr}_t}\right)\frac{\partial T}{\partial x_i}+u_j(\tau_{ij})_{eff}\right] \tag{3}$$

In Eq. (3), the total enthalpy per unit mass H is related to the total energy per unit mass E by $H=E+p/\rho$, where E includes both internal and kinetic energy. In the term representing viscous heating, $(\tau_{ij})_{eff}$ is given as

$$(\tau_{ij})_{eff}=\mu_{eff}\left(\frac{\partial u_j}{\partial x_i}+\frac{\partial u_i}{\partial x_j}\right)-\frac{2}{3}\mu_{eff}\frac{\partial u_i}{\partial x_i}\delta_{ij} \tag{4}$$

where μ_{eff} is the effective viscosity ($=\mu+\mu_t$) and δ_{ij} is the Kronecker delta.

The governing equations are discretized spatially using a fully implicit finite volume scheme, in which the physical domain is subdivided into numerical cells and the integral equations are applied to each cell. The flowfield is represented by associating a distinct value of the discretized solution vector with each control volume, which is then used to evaluate the fluxes at cell faces. The solution vector is computed using a multidimensional linear reconstruction approach (Barth and Jespersen, 1989), which enables higher-order accuracy to be achieved at the cell faces through a Taylor series expansion of the cell-averaged solution vector. The use of a second order accurate scheme makes it feasible to capture the vortex structure and boundary layer flows near wall regions, but only by using fine computational grids. With respect to temporal discretization, an explicit multi-stage time stepping scheme (Jameson et al., 1981) is used to discretize the time derivatives in the governing equations. Then it is assumed that time marching proceeds until a steady state solution is reached.

The standard k-ε turbulence model (Launder and Spalding, 1972), modified to take account of the compressibility effect, is employed to close Eq. (2). The turbulent Mach number used in the dilatation term of the turbulence model is identified as $M_t=(k/a^2)^{0.5}$ (Sarkar and Balakrishnan, 1990). The model for the turbulent viscosity μ_t is written as $\mu_t=\rho C_\mu(k^2/\varepsilon)$, where the turbulent kinetic energy k and dissipation rate ε are solved from the turbulent transport theory. The following model constants are used: $C_\mu=0.09$, $C_{1\varepsilon}=1.44$, $C_{2\varepsilon}=1.92$, $\sigma_k=1.0$ and $\sigma_\varepsilon=1.3$.

3.2 Computational domain and grids

Figure 3 shows the layout of the near-field grids around the present delta wing model and

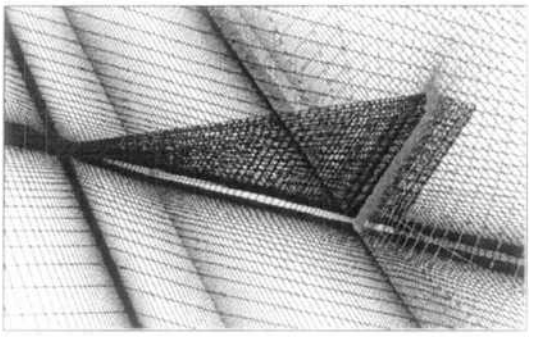

(a) Layout of near-field grids

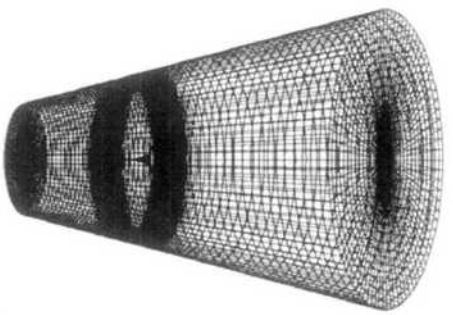

(b) Layout of the entire computational domain

Fig. 3 Computational grid system

the entire computational domain. A three-dimensional structured grid system with about 800,000 nodes was used to simulate vortical flow over the model and node points. The grid size was chosen through the preliminary grid refinement tests to obtain reliable solutions. Grids were clustered in the regions near the wing surfaces and the sharp leading edge where flow separation occured, in order to provide accurate predictions of vortex structures. To obtain domain-independent solutions, external boundaries were extended by the distance of $6c$ (c: chord length) upstream of the apex, $15c$ downstream of the trailing edge and $8c$ spanwise from both sides of the model. For the cases without yaw, especially, computations were conducted only for the right side of the model axis in consideration of symmetry.

3.3 Boundary conditions and analysis

The velocity inlet, pressure outlet and far-field boundary conditions were applied to the upstream boundary, downstream boundary and circumferential boundary respectively, comprising external boundaries of the computational domain. No-slip and adiabatic wall conditions were used for the wing surfaces and the inflow angle at the velocity inlet boundary was changed to simulate the effects of angles of attack and angles of yaw.

For the testing conditions in the present CFD study, the free stream velocity of the delta wing V was changed from 20 m/s to 60 m/s for the cases without yaw at $\alpha=20°\sim28°$, while it was constant at 20 m/s for the cases with $\beta=0°$, 10° and 20° at $\alpha=20°$. The corresponding Reynolds numbers based on the free stream velocity and the wing chord length were about $0.82\times10^6\sim2.47\times10^6$. A convergence criterion of solutions was established when each residual of conservation equations dropped by four orders of magnitude. If the criterion was satisfied and the change in the force coefficient of the delta wing was less than 0.3%, a solution was considered converged.

4. Results and Discussion

4.1 Vortical flow characteristics

Figure 4 shows the static surface pressure distributions of the delta wing model at zero yaw for $\alpha=20°$ and $V=20$ m/s. In order to understand the development of vortical flow, the distributions were obtained at three different chord locations, $x/c=0.3$, 0.6 and 0.8. The computational predictions are given with measured pressure distributions, taken from the past wind tunnel tests (Sohn and Lee, 2002 ; Kim et al., 2003) conducted by KAFA (Korean Air Force Academy). In the figure, C_p is the static pressure coefficient defined by $C_p\equiv(p-p_\infty)/(\rho_\infty V^2/2)$, where p_∞ is the free stream pressure, and the spanwise distance y is normalized by the local semi-span s. As x/c increases, it can be observed that spanwise pressure values decrease with reduced gradient due to diffusion of vortices developed strongly near the leading edge in the chordwise direction. The present computations somewhat underpredict pressure values when compared with the wind tunnel test results but the location of the vortex core, considered to be

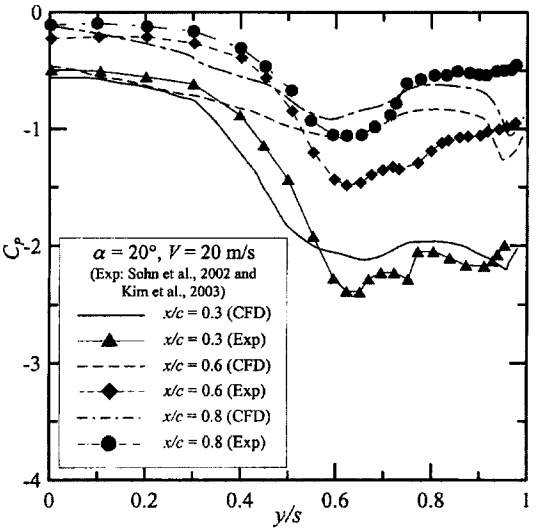

Fig. 4 Wing surface pressure distributions at several chordwise locations (α=20° and V=20 m/s)

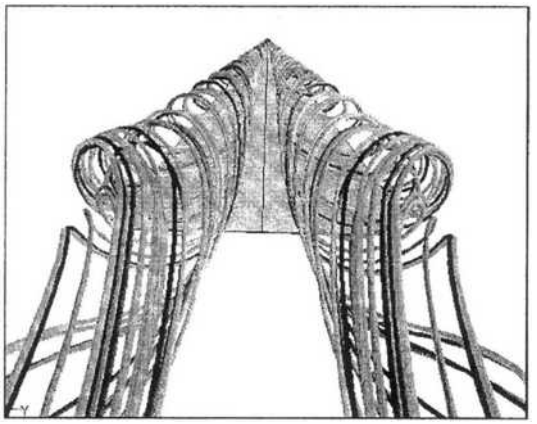

Fig. 5 Path lines over a delta wing (α=20° and V=20 m/s)

present at about y/s=0.6, and the effect of vortex development on the overall flowfield are reasonably predicted. The poor predictions of C_p values in the regions where a vortex pair develops can be attributed to the inability of CFD code to accurately estimate vorticity and coarse grids applied there.

For α=20° and V=20 m/s, Fig. 5 visualizes the behavior of vortices over the present delta wing model through the path lines for the flow

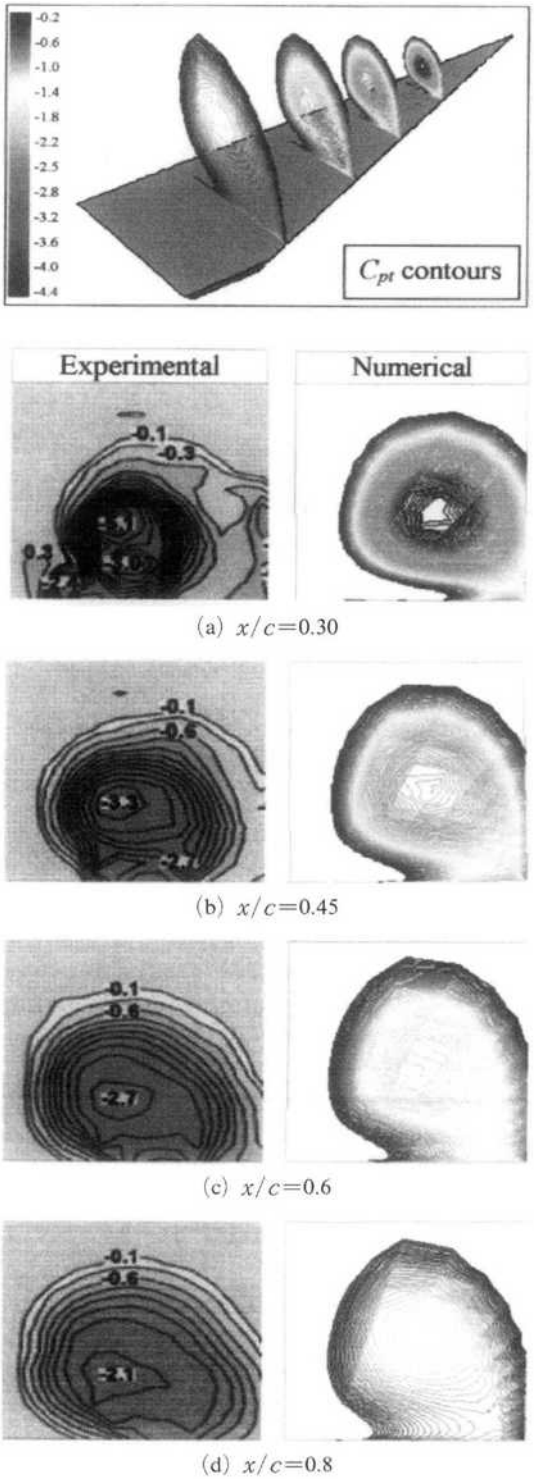

Fig. 6 Total pressure coefficient contours at several chordwise locations (α=24° and V=40 m/s)

particles traced from the sharp leading edge. Strong wake flow develops from the leading edge of the wing due to a large pressure difference between lower and upper surfaces. Then the vortical flow spreads out gradually towards the trailing edge with increased dimensions and consequently breaks down out of the wing surface. The present computational method well predicted a typical subsonic vortical flowfield over a simple delta wing with a sharp edge and the fundamental structure of the vortex system.

Figure 6 shows the total pressure coefficient contours given at several chord locations. The total pressure coefficient C_{pt}, defined by $C_{pt} \equiv (p_t - p_\infty)/(\rho_\infty V^2/2)$, is one of the most useful non-dimensional property to understand the characteristics of vortex structures and it corresponds to a total pressure loss of wake flow. At a chord location close to the trailing edge, C_{pt} of the vortex core is relatively smaller and the wing vortex becomes weaker and more spread. This behavior during the vortex development agrees qualitatively well with the experimental results except the contour in Fig. 6(a), in which the chord location is very close to the wing apex. It is attributed to the insufficient fineness of grids near the leading edge, where very strong vortices can be generated, as reported in past researches (Ekaterinaris and Schiff, 1993 ; Kern, 1993).

4.2 Effect of the free stream velocity and angle of attack

For $\alpha=24°$ and $x/c=0.3$, Fig. 7 shows spanwise pressure distributions on the upper wing surface with a change in the free stream velocity at zero yaw. The computational C_p distributions for $V=20$ m/s, 40 m/s and 60 m/s are presented with the available experimental data (Sohn and Lee, 2002 ; Kim et al., 2003). For all cases, qualitatively good agreement between predicted and measured distributions is observed. As the free stream velocity increases from 20 m/s to 40 m/s, there is about 30% of an increase in the suction pressure peak and the location of the peak value moves outboard by $\Delta y/s \approx 0.07$. It implies that an increase in the free stream velocity introduces an increased vorticity and an outboard

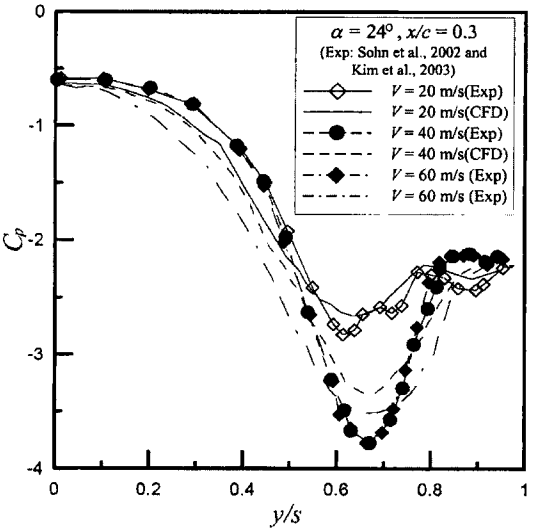

Fig. 7 Wing surface pressure distributions with the free stream velocity ($\alpha=24°$ and $x/c=0.3$)

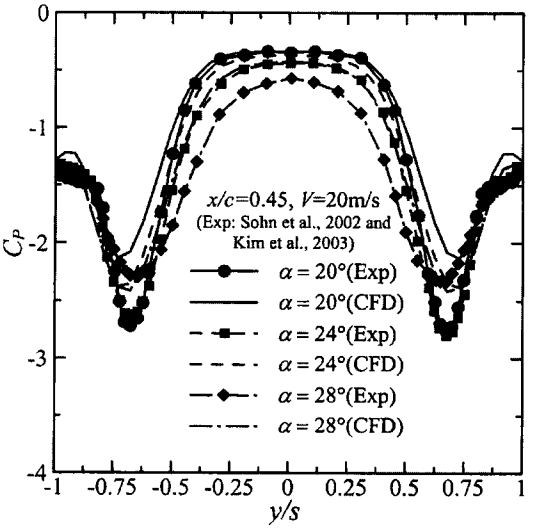

Fig. 8 Wing surface pressure distributions with the angle of attack ($V=20$ m/s and $x/c=0.45$)

movement of the vortex core.

Figure 8 presents the effect of the angle of attack on spanwise pressure distributions for $V=20$ m/s and $x/c=0.45$. For experimental results, as an angle of attack changes from 20° to 24°, the sharp pressure rise inside vortices slightly increases but a further increase in α results in a decreased peak value and relatively weaker

spanwise pressure gradient. It implies that the vortex spreading rate in the chordwise direction may become suddenly high from a certain angle of attack when it is increasing. It is considered that the quantitative deviation between predicted and estimated data can be reduced by using finer grids near the model and improving the turbulence model. As a matter of fact, the Boussinesq approximation (Hinze, 1975) involved in the standard k-ε turbulence model yields a too strong turbulent viscosity in the core of vortices. In the future study, therefore, the turbulence model should be switched to other model such as the Reynolds Stress Model and the Algebraic Reynolds Stress Model that are not based on the Boussinesq approximation. However, the considerations suggested for improving the predictions of vortical flow could be compromised by much higher computational cost.

4.3 Vortical flow over a yawed delta wing

At high angles of attack, the aerodynamic load of delta wings is dominated by the suction pressure acting on the upper wing surface and this pressure is mainly attributed to the strong leading edge vortices developed in leeward regions. Through the C_p distributions in the previous sections, it has been found that intense and concentrated leading edge vortices led to the suction pressure distributions with a high peak value and a large spanwise gradient, while weak and spread leading edge vortices led to those with the opposite features. Through Fig. 9 and Fig. 10, the effect of yaw on aerodynamic load characteristics of the wing model can be understood.

For $\alpha=20°$, $\beta=10°$ and $V=20$ m/s, Fig. 9 shows spanwise pressure distributions at three chord locations, $x/c=0.3$, 0.6 and 0.8, on the upper wing surface. When compared with no-yawed cases in Fig. 4, a yaw angle of 10° completely destroys the symmetry of the vortex pair. As a result, the vortex core on the windward side moves inboard while it on the leeward side moves outboard. Reduced suction pressure peak values at all chord locations implies that an angle of yaw has the vorticity weakened at the given angle of attack. For both no-yawed and

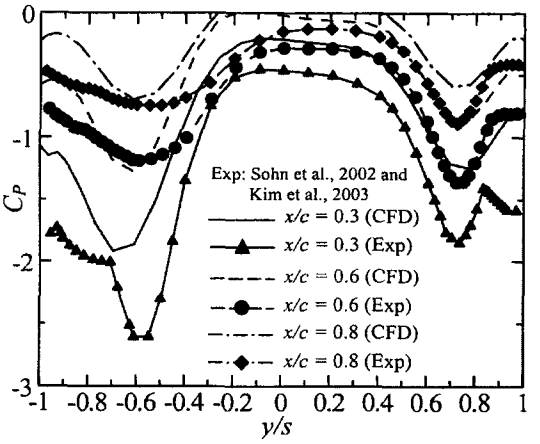

Fig. 9 Wing surface pressure distributions at several chordwise locations ($\alpha=20°$, $\beta=10°$ and $V=20$m/s)

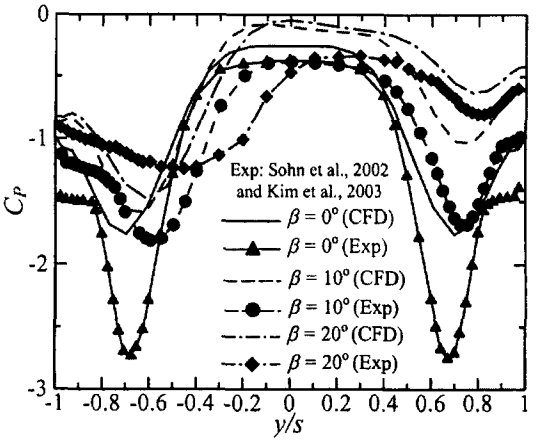

Fig. 10 Wing surface pressure distributions with the angle of yaw ($\alpha=20°$, $V=20$ m/s and $x/c=0.45$)

yawed cases, the changes in the location of the vortex core in the chordwise direction are insignificant.

Figure 10 shows a change in the spanwise pressure distribution with an increased angle of yaw at $\alpha=20°$, $V=20$ m/s and $x/c=0.45$. At $\beta=0°$, no yaw condition, the vortex pair appears completely symmetric and has the highest suction pressure peak. As β increases, the degree of asymmetry becomes larger and the suction pressure peak significantly decreases. Due to the different vortex flow development on both sides

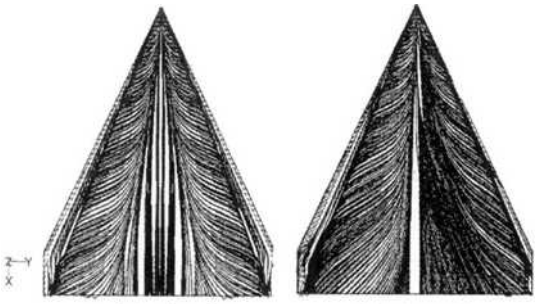

(a) $\beta=0°$ (b) $\beta=10°$

Fig. 11 Computed oilflow pattern of the wing surfaces with and without yaw ($\alpha=20°$ and $V=20$ m/s)

of the wing, at high angles of yaw, the suction pressure peak on the windward side apparently higher than the value on the leeward side. Moreover, with an increased β, the changes in the location of the vortex core and vortex diffusion on the windward side are relatively more significant. The significant C_P deviations observed in Fig. 9 and Fig. 10 are apparently larger than the cases with the zero angle of yaw. In the present computations, a symmetric grid system on the centerline of the wing was used for all testing cases, regardless of the angle of yaw. In this reason, a correct prediction of the displacement of a vortex pair with an angle of yaw could be hardly obtained.

For $\alpha=20°$ and $V=20$ m/s, Fig. 11 presents computed oilflow pattern on the upper surface of the wing model with and without yaw. At $\beta=0°$, the present computational method well predicts the typical subsonic delta wing flow, such as separation and reattachment of the symmetric vortex sheets, as schematically shown in Fig. 1. Due to the effect of yaw, at $\beta=10°$, the reattachment region of the primary vortex is relatively larger while the regions of axially attached flow and the secondary vortex are relatively smaller.

Velocity vectors for $\alpha=20°$ and $V=20$ m/s in Fig. 12 are given at chord locations of $x/c=0.3$, 0.6 and 0.9 in order to understand chordwise vortex development with and without yaw in detail. The vortex core is shown as the center of flow vectors and the vortex diffusion towards

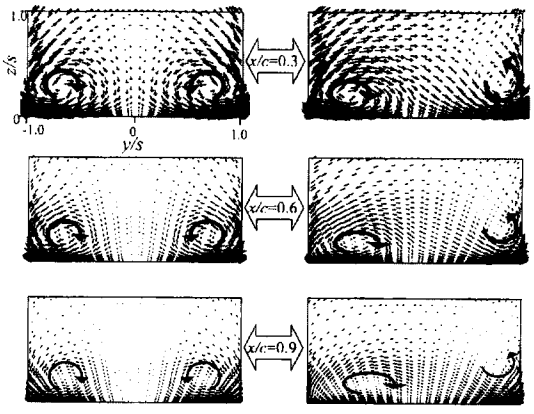

(a) $\beta=0°$ (b) $\beta=20°$

Fig. 12 Velocity vectors of vortical flows at several chordwise locations ($\alpha=20°$ and $V=20$ m/s)

the trailing edge can be clearly observed. The vortex core slightly moves outboard on both sides at $\beta=0°$ while it moves inboard on the windward side and outbord on the leeward side. With an increase in yaw, the vortex core on the leeward side is more significantly shifted away from wing surfaces than on the windward side. In general, larger lift can be obtained as the vortex strength increases and the vortex core is closer to the suction surface. From the figures, it is expected that an increase in the yaw angle will result in a reduction of lift.

5. Conclusions

An understanding of the physics of vortex development and breakdown occurring in vortical flowfields over a delta wing was developed particularly at high angles of attack with and without yaw, using the computational methods. Three-dimensional Navier-Stokes equations with the standard k-ε turbulence model were solved to simulate complex vortical flow characteristics using an implicit finite volume scheme and a multi-stage Runge-Kutta scheme. A flat type wing with a chord of 600 mm and a sweepback angle of 65° were chosen to validate the results obtained through computations with past wind tunnel experiments.

The comparison between predicted and mea-

sured pressure distributions and total pressure coefficient contours showed qualitatively reasonable agreement. The present CFD analysis underpredicted spanwise pressure distributions but well simulated the fundamental structure of the vortex system, chordwise vortex development and aerodynamic load characteristics. Increasing the free stream velocity resulted in an increased vorticity and an outboard movement of the vortex core. At angles of attack, it is expected that the vortex spreading rate in the chordwise direction may increase in view of a decreased spanwise pressure gradient near the vortex core with an increased angle of attack. The results should, however, be improved with finer grids near vortex core regions for better predictions. As the angle of yaw increased, the symmetry of the pair of leading edge vortices was broken. In this situation, the vortex core was largely detached from the suction surface and the vortex strength was decreased.

References

Barth, T. J. and Jespersen, D., 1989, "The Design and Application of Upwind Schemes on Unstructured Meshes," *AIAA Paper* 89-0366.

Ekaterinaris, J. A. and Schiff, L. B., 1990, "Numerical Simulation of the Effects of Variation of Angle of Attack and Sweep Angle on Vortex Breakdown over Delta Wings," *AIAA Paper* 90-3000.

Ekaterinaris, J. A. and Schiff, L. B., 1993, "Numerical Predictions of Vortical Flows over Slender Delta Wings," *J. Aircraft*, Vol. 30, pp. 935~942.

Erickson, G. E., Schreiner, J. A. and Roges, L. W., 1989, "On the Structure, Interaction, and Breakdown Characteristics of Slender Wing Vortices at Subsonic, Transonic, and Supersonic Speeds," *AIAA Paper* 89-3345.

Fujii, K. and Schiff, L. B., 1989, "Numerical Simulation of Vortical Flows over Strake-Delta Wing," *AIAA J.*, Vol. 27, pp. 1153~1162.

Görtz, S., Rizzi, A. and Munukka, K., 1999, "Computational Study of Vortex Breakdown over Swept Delta Wings," *AIAA Paper* 99-3118.

Grismer, D. S., 1995, "Double-Delta-Wing Aerodynamics for Pitching Motions with and without Sideslip," *J. Aircraft*, Vol. 32, pp. 1303~1311.

Hinze, J. O., 1975, *Turbulence*, McGraw-Hill Publishing Co., New York, p. 23.

Hummel, D., 1978, "On the Vortex Formation Over a Slender Wing at Large Angles of Incidence," *AGARD-CPP*-247.

Jameson, A., Schmidt, W. and Turkel, E., 1981, "Numerical Solution of the Euler Equations by Finite Volume Methods Using Runge-Kutta Time-Stepping Schemes," *AIAA Paper* 81-1259.

Ken, C., 1993, "Numerical Study of Blowing on Delta Wings at High Alpha," *J. Aircraft*, Vol. 30, pp. 833~839.

Kern, S. B., 1993, "Vortex Flow Control Using Fillets on a Double-Delta Wing," *J. Aircraft*, Vol. 30, pp. 818~825.

Kim, T. H., Kweon, Y. H., Kim, H. D. and Sohn M. H., 2003, "A Study of the Vortical Flow over a Delta Wing with a Leading Edge Extension," *6th Int. Symposium on Experimental and Computational Aerothermodynamics of Internal Flows*, Shanghai, China, pp. 408~413.

Launder, B. E. and Spalding, D. B., 1972, *Lectures in Mathematical Models of Turbulence*, Academic Press, London, England.

Lee, K. Y. and Sohn, M. H., 2003, "The Vortical Flow Field of Delta Wing with Leading Edge Extension," *KSME Intl. J.*, Vol. 17, pp. 914~924.

Lowson, M. V. and Riley, A. J., 1995, "Vortex Breakdown Control by Delta Wing Geometry," *J. Aircraft*, Vol. 32, pp. 832~838.

Robinson, B. A., Barnett, R. M. and Agrawal, S., 1994, "Simple Numerical Criterion for Vortex Breakdown," *AIAA J.*, Vol. 32, pp. 116~122.

Sarkar, S. and Balakrishnan, L., 1990, "Application of a Reynolds-Stress Turbulence Model to the Compressible Shear Layer," *ICASE Report* 90-18, NASA CR-182002.

Sohn, M. H. and Lee, K. Y., 2002, "Experimental Investigation of Vortex Flow of a Yawed Delta Wing Having Leading Edge Extension," *AIAA paper* 2002-3267.

Verhaagen, N. G. and Naarding, S. H. J., 1989,

"Experimental and Numerical Investigation of the Vortex Flow over a Sidesliping Delta Wing," *J. Aircraft*, Vol. 26, pp. 971~978.

Wentz, W. H. Jr. and Kohlman, D. L., 1971, "Vortex Breakdown on Slender Sharp Edged Wings," *J. Aircraft*, Vol. 8, pp. 156~161.